ACS SyntheticBiology

pubs.acs.org/synthbio

Research Article

Building the Plant SynBio Toolbox through Combinatorial Analysis of DNA Regulatory Elements

Alexander C. Pfotenhauer,[#] Alessandro Occhialini,[#] Mary-Anne Nguyen, Helen Scott, Lezlee T. Dice, Stacee A. Harbison, Li Li, D. Nikki Reuter, Tayler M. Schimel, C. Neal Stewart, Jr, Jacob Beal, and Scott C. Lenaghan*

Cite This: *ACS Synth. Biol.* 2022, 11, 2741–2755

Read Online

ACCESS | Metrics & More | Article Recommendations | Supporting Information

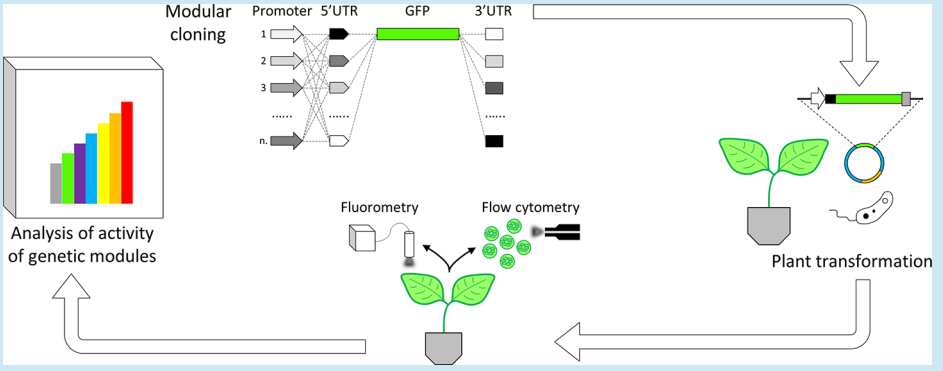

ABSTRACT: While the installation of complex genetic circuits in microorganisms is relatively routine, the synthetic biology toolbox is severely limited in plants. Of particular concern is the absence of combinatorial analysis of regulatory elements, the long design-build-test cycles associated with transgenic plant analysis, and a lack of naming standardization for cloning parts. Here, we use previously described plant regulatory elements to design, build, and test 91 transgene cassettes for relative expression strength. Constructs were transiently transfected into *Nicotiana benthamiana* leaves and expression of a fluorescent reporter was measured from plant canopies, leaves, and protoplasts isolated from transfected plants. As anticipated, a dynamic level of expression was achieved from the library, ranging from near undetectable for the weakest cassette to a ~200-fold increase for the strongest. Analysis of expression levels in plant canopies, individual leaves, and protoplasts were correlated, indicating that any of the methods could be used to evaluate regulatory elements in plants. Through this effort, a well-curated 37-member part library of plant regulatory elements was characterized, providing the necessary data to standardize construct design for precision metabolic engineering in plants.

KEYWORDS: *synthetic biology, transgene expression, genetic regulatory elements, flow cytometry, single-cell analysis, fluorometry*

INTRODUCTION

The growing human population will require an increase in our food production. The effects from climate change will likely affect our ability to grow food, and it will be necessary to improve the resilience of crops to environmental damage.[1] The rise of global temperature linked to severe drought conditions, loss of land due to natural disasters, and emergence of more resilient plant pathogens represent only a few examples of important future agricultural challenges.[2]

Over the last few decades, the role of synthetic biology has become increasingly important to provide alternative solutions to traditional breeding techniques for crop improvement. Many advancements have been achieved for improving crops through the installation of alternative metabolic pathways and high-fidelity enzymes for improved photosynthesis.[3] Additionally, plants have been generated with increased tolerance to biotic and abiotic stresses.[4,5] To improve the nutritional quality of foods, transgenic plants have been developed to increase the level of valuable fatty acids,[6] carotenoids,[7] and anthocyanins[8] and to decrease the level of toxic acrylamide compounds.[9] Despite many of these advancements, the installation of other valuable pathways such as carbon concentrating mechanisms (CCMs) to improve CO_2 fixation[10] and nitrogen-fixing pathways for autonomous atmospheric nitrogen fixation[11] is still at an early stage of research.

Received: March 21, 2022
Published: July 28, 2022

https://doi.org/10.1021/acssynbio.2c00147
ACS Synth. Biol. 2022, 11, 2741–2755

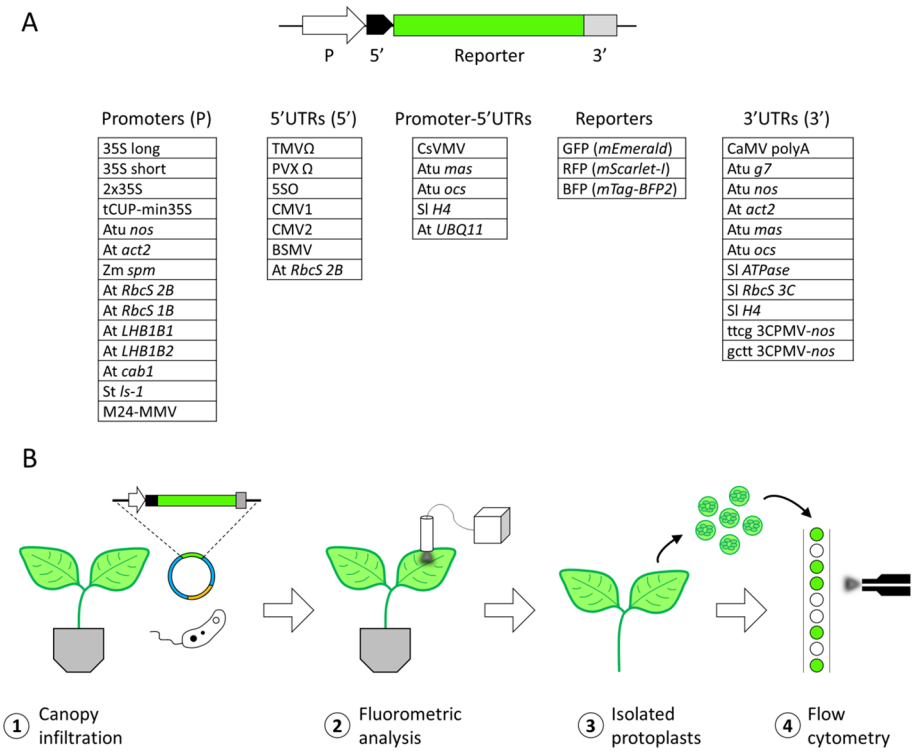

Figure 1. Comparative study of plant genetic regulatory elements. (A) Schematic representation of DNA constructs and regulatory elements used to modulate gene expression in plant cells. Indicated in the image are promoters (P), 5′ untranslated regions (5′UTR), 3′ untranslated regions (3′UTR), and coding sequences for fluorescent protein reporters (reporters). The nucleotide sequences for the regulatory elements and descriptions are provided in Table S1. (B) Schematic representation of the experimental approach used to test genetic elements in plant cells. The approach involves (1) canopy *Agrobacterium tumefaciens*-mediated infiltration of *Nicotiana benthamiana* with DNA constructs, (2) scanning fluorometric analysis of leaf tissue, (3) protoplast isolation from the same tissue, and (4) single cell analysis by flow cytometry.

A fundamental aspect for genetic engineering is the rational design of transformation vectors to reach the targeted spatio-temporal levels of transgene expression. The current plant synthetic biology toolbox comprises endogenous and heterologous genetic elements, as well as synthetic sequences.[12] These genetic elements include promoters and untranslated regions (UTRs) at both 5′ and 3′ ends of the coding region. Transgene expression can be constitutive (in the entire plant or in specific organs and tissues) or induced by treatment with a cognate molecule acting as a genetic switch.[13,14] In association with the core promoter that is involved in transcription initiation, upstream *cis*-regulatory elements (enhancers and silencers) are present in different types, numbers, and orientation. These *cis*-regulatory elements are involved in the modulation of gene expression through binding with particular transcription factors.[15] Both 5′ UTRs, also known as leaders, and 3′ UTRs, also known as terminators, are important sites of post-transcriptional modification. RNA-loop structures of UTRs perform many functions including stability of the resulting transcript. While the presence of 5′ UTRs is important in the formation of an active translation complex, sequences at 3′ are used for transcription termination and stabilization of the resulting mRNA.[16,17]

Many studies have focused on overexpressing transgenes in plant cells for the production of pharmaceutical proteins and other industrially relevant compounds.[18,19] While maximization of expression may be ideal for single enzymes, the installation of complex metabolic pathways requires fine coordination both within the pathway and throughout the plant. With regard to precise metabolic engineering, high expression of all genes is rarely desirable. It is necessary to identify a well-defined part library of regulatory elements that enables tuning of expression to control the optimal stoichiometry of genes necessary to coordinate complex pathways. The part libraries for similar pathway design in microbial systems are much more mature than in plants, as is the standardization of nomenclature across organisms. Further, the throughput of microbial systems allows for combinatorial screening of elements several orders of magnitude greater than what can be accomplished in plants. Quantitative analysis of expression patterns from combinations of plant regulatory elements is critical to enable the breakthroughs envisioned in plant synthetic biology.

High throughput screening in plant cells has been enabled through rapid assembly of transformation vectors through modular cloning,[20] transient expression in model plants, and gene expression quantification. Plant tissues can be analyzed using scanning fluorometry, while single cells (protoplasts) can be analyzed by flow cytometry.[21] Calibration of flow cytometry to units of equivalent standard dye molecules (e.g., molecules of equivalent fluorescein − MEFL) allows reproducible measurements across laboratories.[22,23] This supports better reproducibility of results and improved process debugging by new users. Calibrated measurement also allows estimation of parameters in biologically meaningful units, which has been used with mammalian cells for high accuracy predictive modeling[24] and as a guide for designing improved devices.[25] Here, we use both scanning fluorometry and flow cytometry to quantify transgene expression.

https://doi.org/10.1021/acssynbio.2c00147
ACS Synth. Biol. 2022, 11, 2741−2755

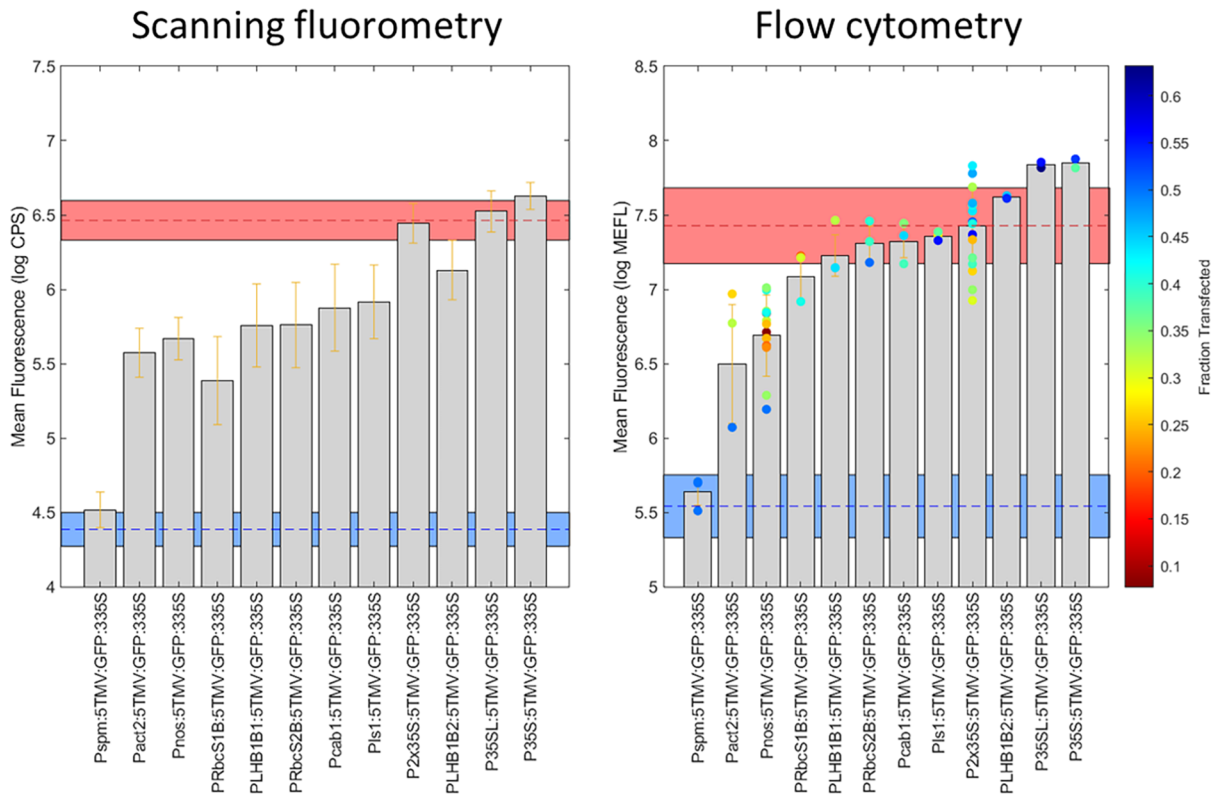

Figure 2. Comparative analysis of promoters. Each construct contains a different promoter (Table S2), while keeping the 5′UTR (TMVΩ leader), reporter gene (GFP), and 3′UTR (35S CaMV polyA) consistent. Graphs represent scanning fluorometry and flow cytometry data obtained using intact leaf tissue and protoplasts isolated from the same tissue. Scanning fluorometry (excitation 475 nm, emission 509 nm) data is expressed as $\log_{10}$ of CPS (counts per second) values, while flow cytometry (excitation 488 nm, emission 510/10 bandpass filter) data is expressed as $\log_{10}$ of MEFL (molecules of equivalent fluorescein) values. Negative (plants transformed with untransformed *Agrobacterium tumefaciens*) and positive (plants transformed with the P2x35S:5TMVΩ:GFP:335S construct) controls are indicated with blue and red lines across the graphs, respectively. Data is represented as the mean ± standard deviation (SD) of at least three transformed plants per construct.

In this work, 91 plant expression cassettes were characterized at the canopy, leaf, and protoplast level to establish an expression library that could be used for tunable metabolic engineering. In particular, regulatory elements were ranked based on the desired expression level and the interplay between regulatory elements and promoters was demonstrated. In many cases, the promoter function was directly tied to pairing with an appropriate 5′ UTR. Further, the importance of careful curation of the parts sequences and the potential effects of minor cloning scars on overall expression are discussed. This characterized library brings plant synthetic biology another step closer toward generating predictive software that can guide construct design from a collection of described parts.

RESULTS AND DISCUSSION

Curation of the Parts Library. The 37-member combinatorial library comprises 14 common plant active promoters, 7 5′UTRs, 11 3′ UTRs, 5 promoter-5′UTR fusions, and 3 fluorescent reporters (Figure 1, Tables S1 and S2). All parts were either obtained from a previously assembled MoClo kit[26] or were produced by gene synthesis. For testing regulatory elements through single expression cassettes, the constructs were subdivided into four different functional groups; promoters, 3′UTRs, promoter-5′UTR fusions, and 5′UTRs. The promoter group was designed to test the activity of promoters, keeping the other regulatory elements of the expression cassette consistent. The 3′UTR group was designed similarly, swapping 3′UTRs while keeping all other elements consistent. The promoter-5′UTR group was designed to test the activity of promoter-5′UTR fusions along with two different 3′UTRs, in all possible combinations. The 5′UTR group was designed to test the activity of 5′UTRs with three different promoters and two different 3′UTRs, in all possible combinations. For all groups tested, a positive control was included (P2x35S:5TMVΩ:GFP:335S). This cassette comprised a 2x35S promoter, a TMVΩ 5′UTR, and a 35S polyA 3′UTR, all of which are commonly used in plant genetic engineering.

The geometric means from individual expression cassettes were compared based on the geometric mean for the reference construct (P2x35S:5TMVΩ:GFP:335S). Analysis of all expression cassettes was conducted on both plant leaves by fluorometry and individual protoplasts by flow cytometry. By analyzing the same sample at the population and individual cell level, it was possible to determine the strengths and limitations of each analytical approach.

Investigating the Effect of the Promoter Region. Cassettes using the viral CaMV 35S promoters enable higher expression of the reporter gene compared to both the *nos* promoter from *Agrobacterium tumefaciens* and most other endogenous plant promoters tested. Out of the three 35S promoters tested, cassettes using the short (−420 to +6) and long (−1332 to +6) promoters generated the highest levels of reporter gene expression (Figure 2). The strong activity of the 35S promoters is compatible with previous investigations demonstrating that the upstream −343/−46 region is

https://doi.org/10.1021/acssynbio.2c00147
ACS Synth. Biol. 2022, 11, 2741−2755

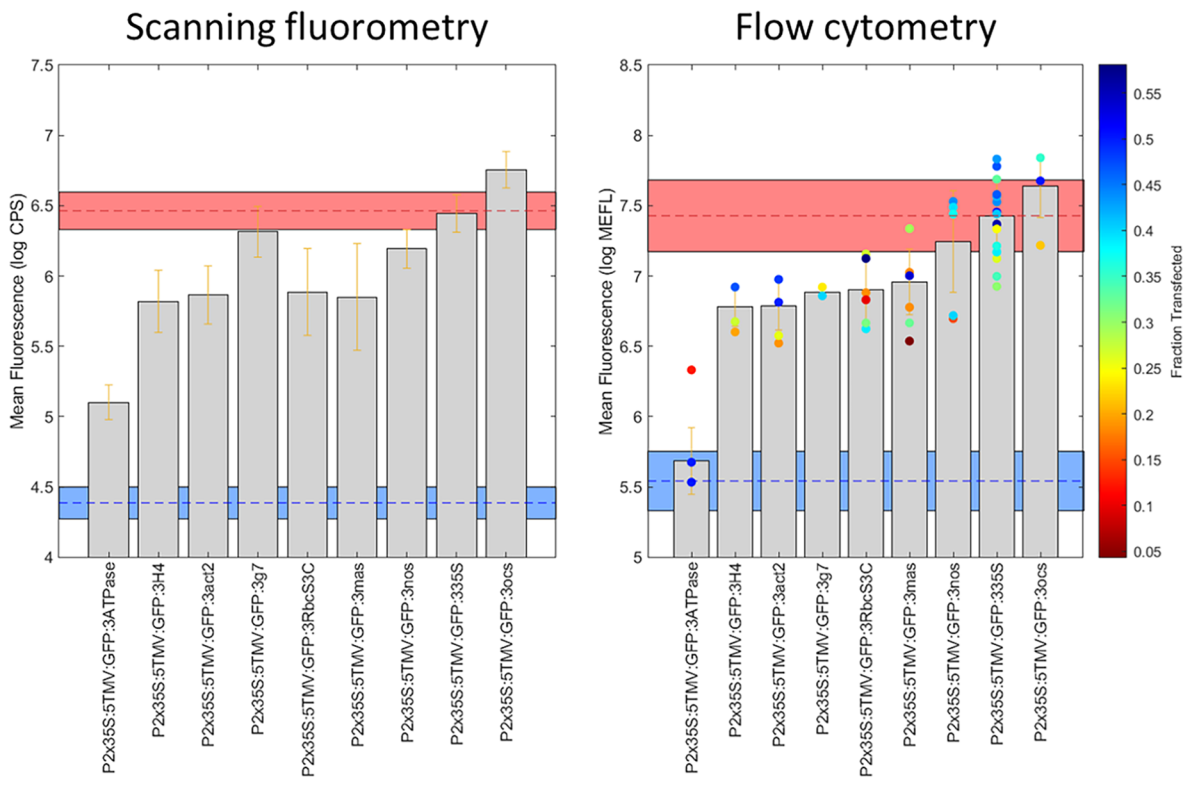

Figure 3. Comparative analysis of 3′UTRs. Each construct contains a different 3′UTR (Table S2), while keeping the promoter (CaMV 2x35S), 5′UTR (TMVΩ leader) and reporter gene (GFP) consistent. Graphs represent scanning fluorometry and flow cytometry data obtained using intact leaf tissue and protoplasts isolated from the same tissue. Scanning fluorometry (excitation 475 nm, emission 509 nm) data is expressed as $\log_{10}$ of CPS (counts per second) values, while flow cytometry (excitation 488 nm, emission 510/10 bandpass filter) data is expressed as $\log_{10}$ of MEFL (molecules of equivalent fluorescein) values. Negative (plants transformed with untransformed *Agrobacterium tumefaciens*) and positive (plants transformed with the P2x35S:5TMVΩ:GFP:335S construct) controls are indicated with blue and red lines across the graphs, respectively. Data is represented as the mean ± standard deviation (SD) of at least three transformed plants per construct.

responsible for the majority of promoter strength.[27,28] Surprisingly, both of the single versions of the 35S promoters regulated expression at approximately half a decade higher than the positive control P2x35S:5TMVΩ:GFP:335S. This is in contrast with early publications from 1987 that demonstrated that duplication of enhancer sequences has a considerable effect in improving promoter strength.[29,30] However, the 35S annotated in one of these publications contains three SNPs in the distal region of the promoter, and this distal region is thought to activate the core promoter.[30] Differences in activity from these initial studies could also be due to the different lengths of duplicated regions (−148/−89 vs −343/−89), cloning artifacts, or the use of different UTRs. More recently, it was shown that the three 35S promoters used in our study have similar activity when quantified at the GFP level.[26]

Other than the monocotyledon *spm* promoter that is not active in dicotyledon plants, cassettes using all other promoters tested provided a detectable range of expression by both scanning fluorometry and flow cytometry. The flow cytometry data suggested that the endogenous plant promoters *LHB1B2*, *ls1*, *cab1*, *RbcS2B*, and *LHB1B1* regulated expression at a similar level to P2x35S:5TMVΩ:GFP:335S. Again, this result is surprising considering the generally accepted dogma that the 2x35S promoter is the best promoter for high level transgene expression. Cassettes using promoters from *RbcS1B*, *act2*, and *nos* (−256 to +20) expressed at the weakest level, at a half decade to a decade lower than P2x35S:5TMVΩ:GFP:335S. The majority of endogenous promoters have complex and non-fully characterized structures of upstream *cis*-regulatory elements, making their activity unpredictable in different environmental conditions. Therefore, the plant genetic engineering toolbox will benefit greatly from rational deconstruction of endogenous promoters, with the ultimate goal of building synthetic promoters that reach desired levels of either constitutive, inducible, or organ specific activity.[31,32]

Investigating the Effect of the 3′UTR Region. Even with a strong promoter/5′UTR combination (P2x35S:5TMVΩ), the choice of 3′UTR has a strong effect on gene expression (Figure 3). Cassettes with the *A. tumefaciens ocs* 3′UTR were the strongest, expressing at a similar level to the P2x35S:5TMVΩ:GFP:335S cassette and cassettes with the *nos* 3′UTR. While scanning fluorometry indicated that the *g7* 3′UTR may positively enhance expression, flow-cytometry data did no support this trend. Constructs using the *mas* 3′UTR reduced expression approximately half a decade, while *RbcS3C*, *g7*, *act2*, and *H4* 3′UTRs showed similar activities, all reducing expression to a similar level compared to P2x35S:5TMVΩ:GFP:335S. The most significant reduction in reporter expression was observed for the 3′UTR from the endogenous plant *ATPase*, which could not be resolved from the background signal in the flow cytometry analysis.

As shown in previous investigations, this work supports the hypothesis that choosing the appropriate 3′UTR is necessary for reaching optimal transgene expression in plant cells.[33] The modulation of the 3′UTR allows an additional level of

https://doi.org/10.1021/acssynbio.2c00147
ACS Synth. Biol. 2022, 11, 2741−2755

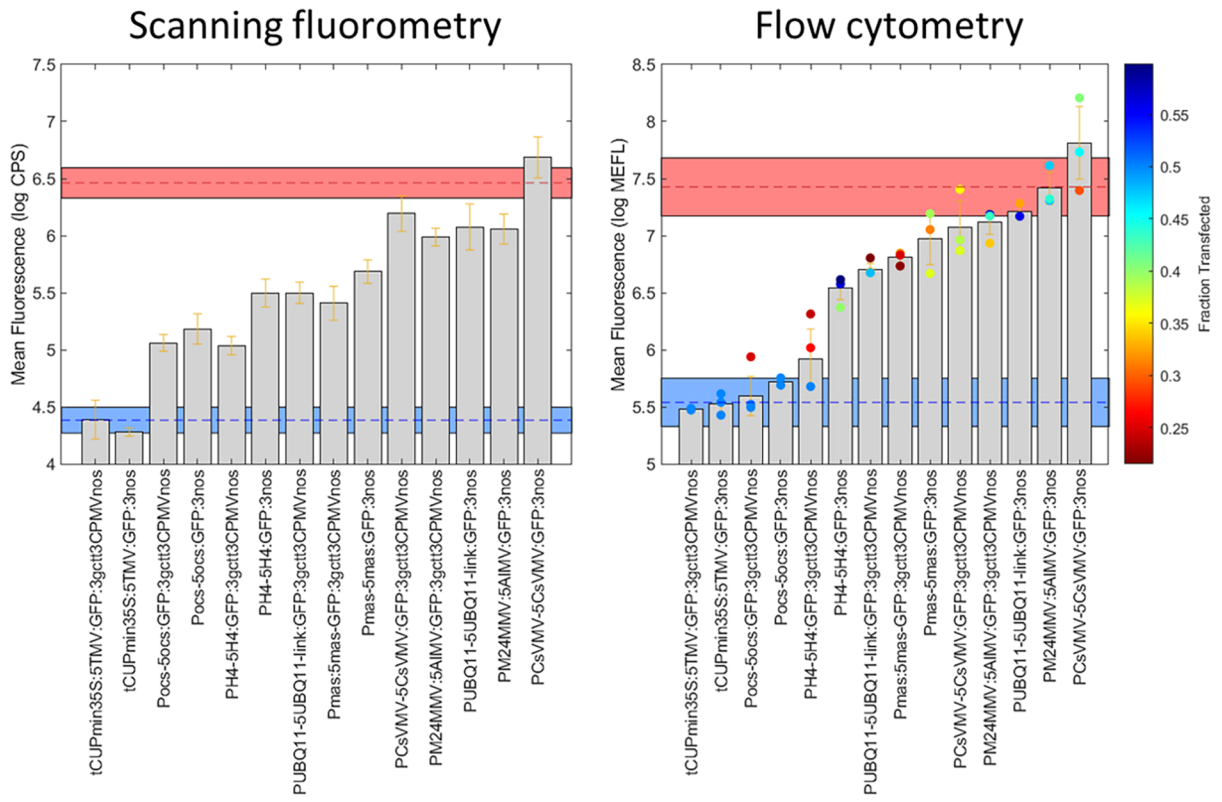

Figure 4. Comparative analysis of promoter-5′UTR fusions in combination with 3′UTRs of different activities. Each construct contains a different promoter-5′UTR (Table S2). While the reporter gene (GFP) was kept consistent, two different 3′UTRs (*nos* 3′UTR and gctt3CPMV-*nos* fusion) were interchanged downstream from each promoter-5′UTR fusion. Graphs represent scanning fluorometry and flow cytometry data obtained using intact leaf tissue and protoplasts isolated from the same tissue. Scanning fluorometry (excitation 475 nm, emission 509 nm) data is expressed as $\log_{10}$ of CPS (counts per second) values, while flow cytometry (excitation 488 nm, emission 510/10 bandpass filter) data is expressed as $\log_{10}$ of MEFL (molecules of equivalent fluorescein) values. Negative (plants transformed with untransformed *Agrobacterium tumefaciens*) and positive (plants transformed with the P2x35S:5TMVΩ:GFP:35S construct) controls are indicated with blue and red lines across the graphs, respectively. Data is represented as the mean ± standard deviation (SD) of at least three transformed plants per construct.

stoichiometric control for a multi-component pathway. The cassettes using the *ocs*, 35S, and *nos* 3′UTRs were the strongest tested. Unlike *ocs*, other commonly used 3′UTRs reported in the literature, such as *mas*, *RbcS3C*, *g7*, *act2*, and *H4*[26,34,35] reduced the cassette expression level, representing suboptimal modules for transgene overexpression applications. However, with regard to modulating transgene expression, these 3′UTRs could be useful to reduce expression from cassettes using strong predetermined promoters/5′UTRs.

In addition to demonstrating the importance of the 3′UTR with regards to gene expression/translation, comparison of the fluorometry and flow cytometry data for the *ATPase* 3′UTR expression cassette revealed a limitation of the current flow cytometry assay. While reporter gene expression could not be resolved from the flow cytometry assay, it could be clearly resolved in the fluorometry analysis. At first, this result was confounding as flow cytometry is far more sensitive than fluorometry; however, upon further examination of the fluorometry data, it was determined that the relatively low ratio of transformed to untransformed cells made it more difficult to resolve low expressing constructs than fluorometry. This could be due to several technical considerations of the current protoplast flow cytometry assays. (1) Transformed protoplasts may have weakened plasma membranes compared to untransformed protoplasts and thus are more sensitive to shear forces within the flow cells; and (2) protoplasts are near the size maximum for many flow cytometers and are inherently susceptible to shearing through the microfluidic nozzles. Imaging data collected prior to flow cytometry support the hypothesis that a significant portion of cells are sheared as a result of the microfluidic environment resulting in an overall decreased signal. Further optimization of the flow cytometry protocol will likely be necessary to increase the resolution of flow cytometry analysis. In the current work, the ability to directly compare the flow cytometry and leaf fluorometry allowed us to resolve all levels of expression.

Investigating the Effect of Promoter-5′UTR Fusion Regions. In addition to the characterization of 5′UTR modules fused to well-characterized promoters (Figure 2), constructs were designed to test other promoter-5′UTR fusions found in the literature (Figure 4). These regulatory elements were tested in combination with either *nos* or gctt-3CPMV-*nos* 3′UTRs. Except for the nonfunctional *Nicotiana tabacum* cryptic promoter tCUP fused to the minimal promoter/5′UTR region min35S::TMV Ω, all other cassettes tested showed a range of detectable activity. The CsVMV promoter-5′UTR fusion regulated expression at the highest level in this group of constructs, at nearly half a decade over P2x35S:5TMVΩ:GFP:35S. This is in agreement with several previous investigations that showed higher activity from the CsVMV promoter compared to 35S in several plant systems.[36,37] The flow cytometry data suggests that the viral PM24 MMV promoter fused to the AlMV 5′UTR regulates expression at a lower level from the CsVMV fusion, though at

https://doi.org/10.1021/acssynbio.2c00147
ACS Synth. Biol. 2022, 11, 2741−2755

the same level as P2x35S:5TMVΩ:GFP:335S. The UBQ11 promoter-5′UTR cassette drove the highest level of reporter expression from the endogenous plant promoter-5′UTR fusions, also at the same level as P2x35S:5TMVΩ:GFP:335S. The UBQ11 promoter is one of few identified strong endogenous plant promoters commonly used in genetic engineering.[38] Considering that viral sequences can induce transcriptional silencing of transgenes,[39] the use of strong endogenous plant promoters has a distinct advantage for building engineered plants. Among the others tested, the cassette using the *mas* promoter-5′UTR reduced expression by approximately half a decade and the *H4* cassette by a full decade, and the *ocs* cassette only generated signal close to the background level. As seen in Figure 2, low expressing cassettes such as Pocs-5ocs:GFP:3gctt3CPMV*nos* and Pocs-5ocs:GFP:3*nos* are undetectable by flow cytometry, though they show detectable expression by scanning fluorometry. It is interesting that using the *ocs* promoter-5′UTR decreases cassette expression, while the *ocs* 3′UTR greatly increases cassette expression (Figure 4).

Independent of the testing of activity from all promoter-5′UTR combinations, the use of two 3′UTRs with different strengths resulted in the same high and low trend of expression regulation. For these 5′UTR/3′UTR pairings, there was no substantial interaction between the upstream promoter-5′UTR and the downstream 3′UTR, as the addition of the weak 3′UTR (gctt-3CPMV-*nos*) decreased expression levels for all promoter-5′UTR cassettes tested by approximately half a decade. Thus, with these elements, the dynamic range of expression achieved by varying the 5′UTR was considerably larger than when varying the 3′UTR. It should be noted that comprehensive analysis of a library of 5′UTR/3′UTR pairings may reveal that certain pairings have either an antagonistic or synergistic effect on gene expression. Further study on the relationship between these elements in plant gene expression is clearly warranted and will help inform cassette design.

Investigating the Effect of the 5′UTR Region. We next modulated expression by changing both the 5′ and 3′UTRs, while keeping one of three promoter sequences consistent (Figure 5). The *nos* promoter cassettes expressed at a reduced level compared to both 35S and 2x35S for all combinations tested. As *nos* is one of the weakest available plant active promoters, many of the cassettes were undetectable by flow cytometry. Scanning fluorometry data suggests that the TMV 5′UTR cassette was the weakest, expressing at approximately a decade and a half below P2x35S:5TMVΩ:GFP:335S, followed by BSMV, 5SO, and PVX at slightly higher levels. The CMV2, *RbcS2*, and CMV1 cassettes all expressed at approximately one decade below P2x35S:5TMVΩ:GFP:335S.

Cassettes using the 35S promoter and all 5′UTRs other than TMV expressed at a similar level to P2x35S:5TMVΩ:GFP:335S, while TMV reduced expression by approximately half a decade. Absence of a 5′UTR reduced expression by a full decade. Interestingly, cassettes using the 2x35S promoter and the PVX 5′UTR expressed approximately half a decade higher than P2x35S:5TMVΩ:GFP:335S. This is especially interesting considering that the addition of the PVX 5′UTR to the *nos* promoter greatly reduced expression. The BSMV 5′UTR reduced expression slightly, and the absence of a 5′UTR reduced expression by approximately half a decade, while all others expressed at a similar level to P2x35S:5TMVΩ:GFP:335S.

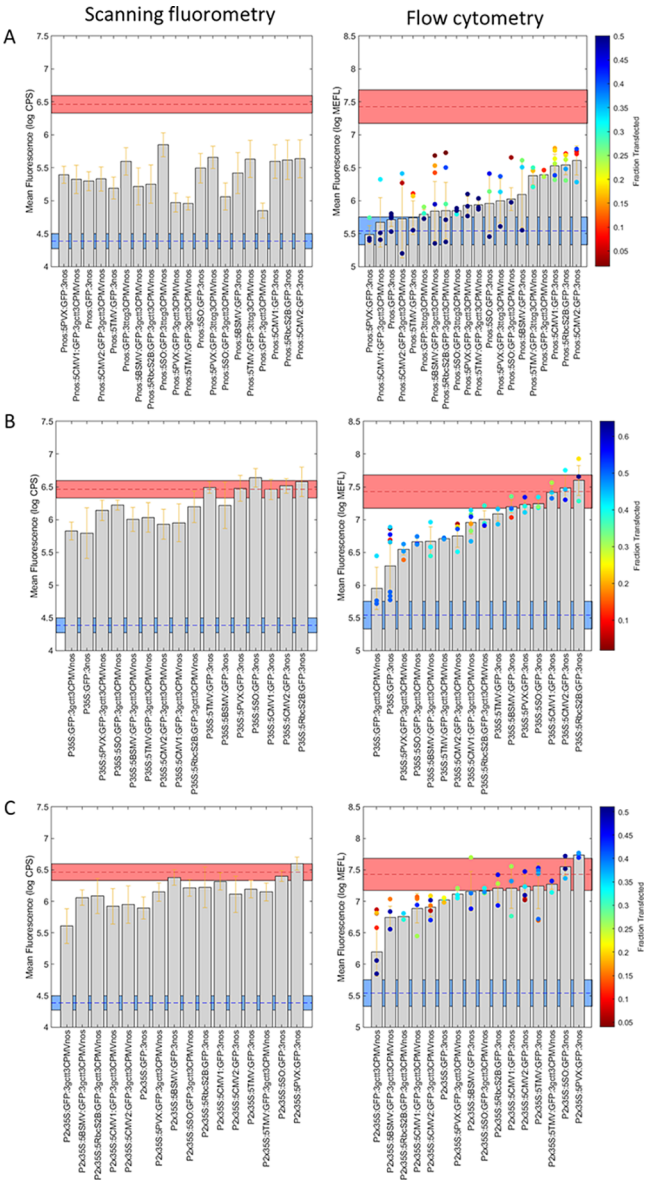

Figure 5. Comparative analysis 5′UTRs in combination with promoters and 3′UTRs of different activities. Per promoter group (*nos*, 35S and 2x35S, in A-C, respectively), the library of 5′UTRs (Table S2) was tested along with two 3′UTRs (*nos* 3′UTR and gctt3CPMV-*nos* fusion) while keeping the reporter gene (GFP) consistent. The promoter *nos* was also tested with or without three 5′UTRs (TMVΩ, PVXΩ and 5SO) along with a 4 bp (ttcg) variant of 3CPMV-*nos* 3′UTR (ttcg3CPMV-*nos*). Graphs represent scanning fluorometry and flow cytometry data obtained using intact leaf tissue and protoplasts isolated from the same tissue. Scanning fluorometry (excitation 475 nm, emission 509 nm) data is expressed as $\log_{10}$ of CPS (counts per second) values, while flow cytometry (excitation 488 nm, emission 510/10 bandpass filter) data is expressed as $\log_{10}$ of MEFL (molecules of equivalent fluorescein) values. Negative (plants transformed with untransformed *Agrobacterium tumefaciens*) and positive (plants transformed with the P2x35S:5TMVΩ:GFP:335S construct) controls are indicated with blue and red lines across the graphs, respectively. Data is represented as the mean ± standard deviation (SD) of at least three transformed plants per construct.

The activity of all promoters was improved by adding 5′UTRs, confirming the importance of this element when designing genetic constructs. The 5′UTR is crucial for stabilizing transcripts, which positively enhances gene ex-

https://doi.org/10.1021/acssynbio.2c00147
ACS Synth. Biol. 2022, 11, 2741−2755

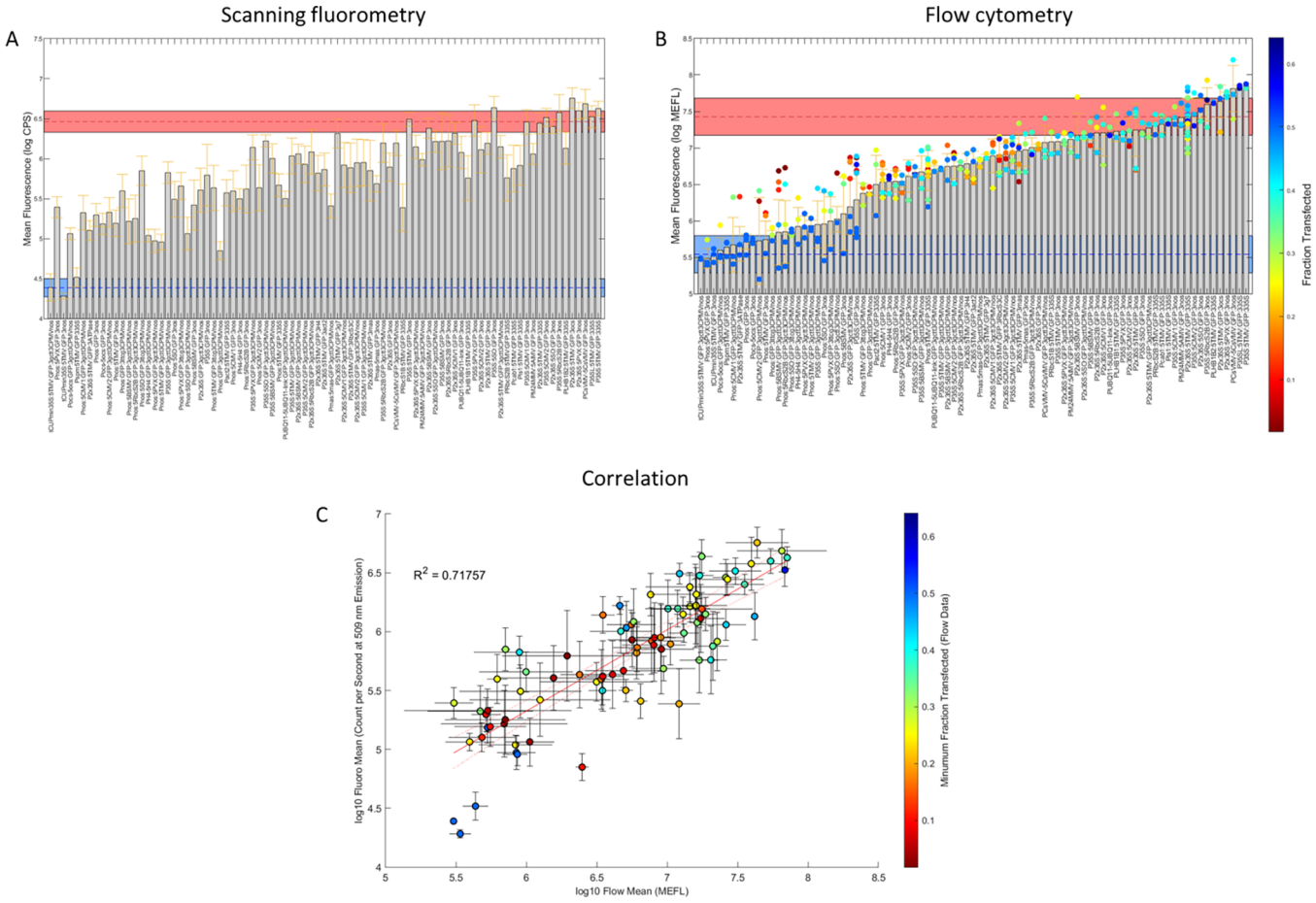

Figure 6. Comparison of scanning fluorometry and flow cytometry data for all combinations of genetic regulatory elements. (A, B) Graphs represent scanning fluorometry and flow cytometry data obtained using intact leaf tissue and protoplasts isolated from the same tissue. Scanning fluorometry (excitation 475 nm, emission 509 nm) data is expressed as $\log_{10}$ of CPS (counts per second) values, while flow cytometry (excitation 488 nm, emission 510/10 bandpass filter) data is expressed as $\log_{10}$ of MEFL (molecules of equivalent fluorescein) values. Negative (plants transformed with untransformed *Agrobacterium tumefaciens*) and positive (plants transformed with the P2x35S:5TMVΩ:GFP:335S construct) controls are indicated with blue and red lines across the graphs, respectively. Data is represented as the mean ± standard deviation (SD) of at least three transformed plants per construct. (C) Graph showing the correlation between scanning fluorometry measurements and flow cytometry data. The R^2 correlation value of ∼0.72 is shown in the graph.

pression.[40,41] However, the degree of increased expression was not consistent between the promoters. These results suggest that the addition of 5′UTRs affects promoter activity differently, and expression from combinations may not be easily predicted. The enhancer effect of 5′UTRs is not always linked to the presence of common motifs in their sequence,[42] supporting the hypothesis that the upstream promoter region may have a synergistic role. Therefore, testing combinations of heterologous promoters and 5′UTRs is an important aspect to consider when designing transgene expression cassettes. Similarly to what is observed in Figure 4, the effect on activity from different 3′UTRs appears to be distinct from the upstream sequences. The addition of the weak gctt-3CPMV-*nos* repeatedly decreased activity as compared to the *nos* 3′UTR.

Common Four Base Pair Scar (GCTT) between the Stop Codon and the 3′UTR Reduces the Cassette Expression Level. In order to test the effect of short base pair sequences introduced as cloning scars between regulatory elements, the activity of two different four base pair 3CPMV-*nos* 3′UTRs were tested downstream of four different *nos* promoter/5′UTR fusions (5SO, PVX, TMVΩ, or absence of 5′UTR). For this purpose, either the commonly used GCTT[20,26] or TTCG 3′ scar was inserted between the GFP stop codon and the 3CPMV-*nos* 3′UTR (Figure 5A and Table S2). These two groups were compared to constructs with the *nos* 3′UTR. Scanning fluorometry data suggested that cassettes using the gctt-3CPMV-*nos* reduced expression for all 5′UTRs tested by approximately one and a half decades compared to P2x35S:5TMVΩ:GFP:335S. The use of the *nos* 3′UTR decreased cassette expression by approximately one and a half decades for all 5′UTRs tested. Cassettes with ttcg-3CPMV-*nos* expressed at the highest levels, at approximately one decade under P2x35S:5TMVΩ:GFP:335S for the 5SO, PVX, TMV, or absence of 5′UTR. As expected due to low expression values, flow cytometry was not able to validate differences between these cassettes.

Due to the consistent change in expression using GCTT or TTCG 3′ overhangs, we generated 10 additional constructs by swapping the four base pairs between GCTT and TTCG either one, two, three, or four nucleotides at a time (Figure S1). All constructs contained the *nos* promoter, TMVΩ 5′UTR, and 3CPMV-*nos* 3′UTR. The construct using the GTTT overhangs expressed at the lowest ranked level, which was similar to

https://doi.org/10.1021/acssynbio.2c00147
ACS Synth. Biol. 2022, 11, 2741−2755

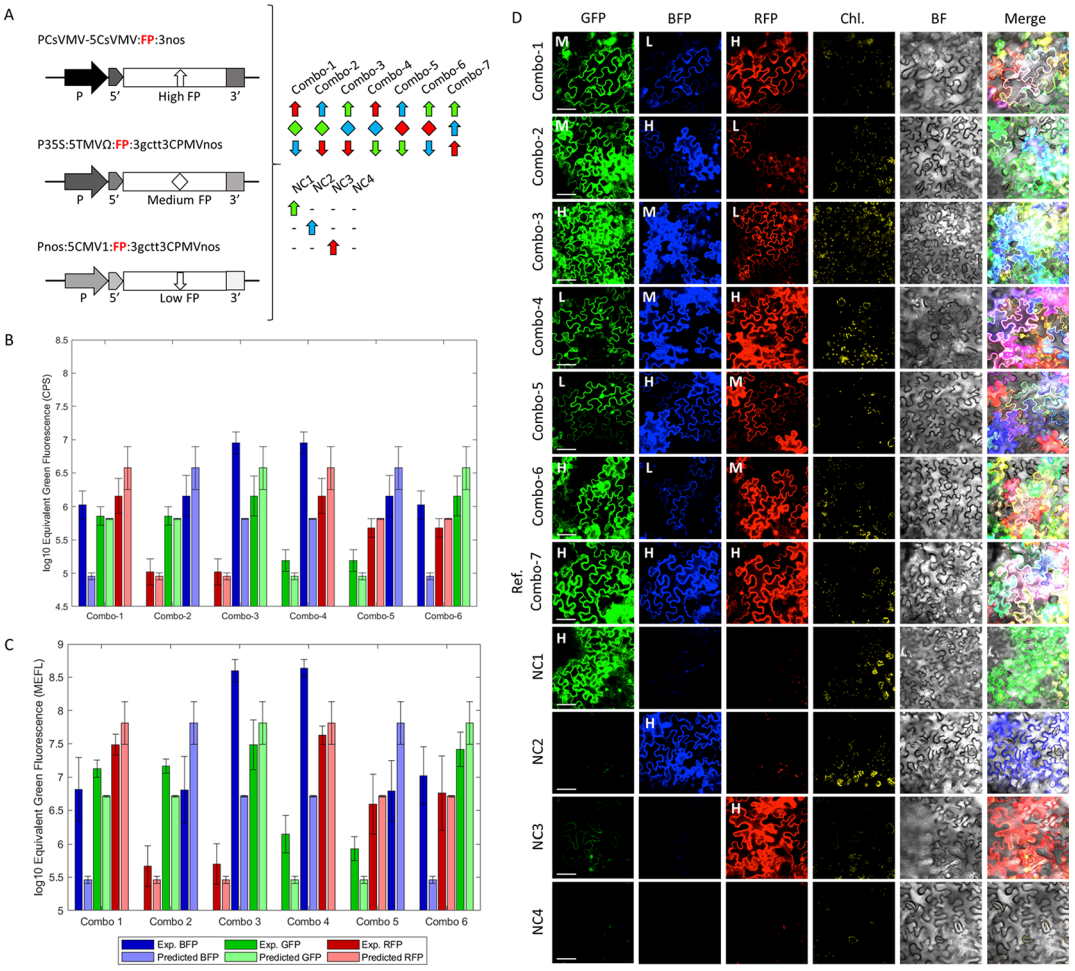

Figure 7. Combining transgene cassettes to achieve predicted fluorescence levels within a three-gene pathway. (A) High (PCsVMV-5CsVMV:FP:3*nos*, H), medium (P35S:5TMVΩ:FP:3gctt3CPMV*nos*, M), and low (P*nos*:5CMV1:FP:3gctt3CPMV*nos*, L) regulatory element cassettes (Table S2) were designed to control the expression of either GFP, BFP, or RFP reporters in all possible combinations. Combination 1 (Combo-1): H RFP, M GFP, and L BFP; combination 2 (Combo-2): H BFP, M GFP, and L RFP; combination 3 (Combo-3): H GFP, M BFP, and L RFP; combination 4 (Combo-4): H RFP, M BFP, and L GFP; combination 5 (Combo-5): H BFP, M RFP, and L GFP; combination 6 (Combo-6): H GFP, M RFP, and L BFP. (B, C) Graphs represent scanning fluorometry and flow cytometry data obtained using intact leaf tissue and protoplasts isolated from the same tissue. Scanning fluorometry (excitation 475, 550, and 400 nm, emission 509, 574, and 455 nm) data is expressed as $\log_{10}$ of CPS (counts per second) values, while flow cytometry (excitation 488, 561, and 405, emission 510/10, 585/16, and 440/50 bandpass filters) data is expressed as $\log_{10}$ of MEFL (molecules of equivalent fluorescein) values for GFP, RFP, and BFP respectively.. Negative (plants transformed with untransformed *Agrobacterium tumefaciens*) and positive (plants transformed with the P2x35S:5TMVΩ:GFP:3*35S* construct) controls are indicated with blue and red lines across the graphs, respectively. Data is represented as the mean ± standard deviation (SD) of at least three transformed plants per construct. The fluorescence levels of combinations 1−6 are compared with predicted single cassette fluorescence levels (light green, blue, and red). (D) Confocal images showing the same epidermal *N. benthamiana* leaf cells transformed with the indicated construct combinations, (Combo-1−6); reference combination 7 (Combo-7): H GFP, H RFP, and H BFP; negative control 1 (NC1): H GFP only; negative control 2 (NC2): H BFP only; negative control 3 (NC3): H RFP only; and negative control 4 (NC4): leaves transformed with wild-type *A. tumefaciens*. Chlorophyll (Chl), bright-field (BF), and merged images are indicated. Scale bars = 50 μm.

GCTT. The highest ranked construct used the TTCG overhangs. Interestingly, all six overhangs tested that began with a G nucleotide were the lowest ranked, while all six overhangs beginning with a T were the highest ranked.

All combinations indicated a strong change of expression levels due to the presence of different four base pair scars. The ttcg-3CPMV-*nos* consistently increased activity, while the gctt-3CPMV-*nos* decreased activity compared to constructs with the *nos* 3′UTR. Surprisingly, these results indicate that cloning scars are a critical aspect to consider when designing expression cassettes. It is possible that the intrinsic secondary loop-structure and stability of the transcript can be altered through the introduction of a few base pairs outside of the main 3′UTR sequence. This is supported by a previous study performed using the 3′UTR of CPMV RNA-2, which demonstrated that the preservation of an optimal RNA secondary structure was fundamental to achieve high expression.[17] In this study, the introduction of either point mutations in critical RNA-Y-loops within the 3CPMV, or the introduction of a linker in between two 3′UTRs (3CPMV and *nos*) had a strong effect on the gene expression level.[17]

Our data added one more level of complexity for using 3′UTR modules, demonstrating that even changing a few base pairs can decrease the cassette expression level. The introduction of scars in between regulatory elements is part of both traditional and Golden Gate cloning, and therefore choosing appropriate restriction sites and overhangs is fundamental for optimal construct design. With regards to

https://doi.org/10.1021/acssynbio.2c00147
ACS Synth. Biol. 2022, 11, 2741−2755

Golden Gate cloning, the GCTT sequence is a common 3′ overhang used to design gene of interest modules in many plasmid kits.[20,26] Therefore, reconsidering the use of this particular overhang and testing alternative sequences is particularly important to achieve high transgene expression in plant cells. As important is the need to identify insulator regions that can minimize the effects of scars on expression. A previous work in *E. coli* promoters demonstrated a path for using randomized insulators to reduce the impact of scars on gene expression.[43] Similar designs for plant constructs may help alleviate this issue to increase the fidelity of engineered plants.

Ranking Genetic Regulatory Elements to Achieve Different Activity Levels. In addition to the investigation of regulatory elements in various groupings, the activity of all constructs was ranked against one another (Figure 6). The graph showing the expression of all 85 GFP expressing constructs vs P2x35S:5TMVΩ:GFP:35S reflects a wide range of expression levels. Expression ranges from undetectable when using the nonfunctional tCUP promoter (two decades below), to very high levels when using the CsVMV promoter (approximately half a decade above). For a number of commonly used regulatory elements, plant genetic engineering is largely devoid of clear sequence information and common nomenclature for elements used in different laboratories. To further this issue, it is not uncommon for distinct elements to be identified with the same name. In our library, three different 35S promoters found in common databases have been characterized: the short 35S promoter from the CaMV virus, a longer and mutated form, and a repeated double form. The three versions might casually be referred to as 35S, though they may differ in activity strength, especially when used with various 5′UTRs (Figures 2 and 2). While the greater synthetic biology community has begun to use standardization of parts nomenclature through software solutions, such as SBOL,[44] there is currently no extensive effort to solve this stopgap in plant synthetic biology. Additionally, the effects from small four base pair scars clearly play a discernible role in transgene expression and should not be overlooked (Figure 5C and Figure S1). Often, plasmids may be casually interchanged within laboratories, and small differences between commonly used regulatory elements may be overlooked. This data demonstrates that deep sequence analysis of genetic modules used for transgene expression is fundamental to achieve rational construct design. This is particularly important to study regulatory elements where small mutations in critical functional regions could drastically affect their activity.[17,32]

Combining Transgene Cassettes to Achieve Predicted Level of Expression within a Three-Gene Pathway. As a proof of concept to demonstrate the ability to modulate the stoichiometry of gene expression within a three-component pathway, plant cells were co-transformed with low, medium, and high combinations of regulatory elements to express GFP, RFP, or BFP reporter cassettes in all possible combinations (Combo-1−6) (Figure 7). Values obtained from both leaves and single cell analyses were converted from RFP or BFP units into equivalent GFP units using values from plants co-transfected with three high-expressing constructs controlling the three reporters. If the regulatory elements can be applied equivalently to different coding sequences and the expression cassettes do not interfere significantly with one another, then we would predict that the expression levels from each color in these three-color constructs should be close to the expression levels of the single-color GFP constructs reported above. The observed results are shown in Figure 7A−C. Signal specificity and absence of cross contamination between the three fluorescent channels was confirmed by confocal microscopy (Figure 7D). For the GFP cassettes, the combinations expressed as expected, with low values obtained from Combo-4 and Combo-5, medium values from Combo-1 and Combo-2, and high values from Combo-3 and Combo-6. Interestingly, predicted values from flow cytometry for medium and low expressing cassettes were slightly less than those achieved from the combinations, while the values predicted for the high expressing cassette were slightly greater than those of the combination. A similar trend was seen for the RFP cassettes. The low, medium, and high expressing combinations expressed as expected. As with the GFP cassettes, the predicted values for the low RFP expressing cassettes were slightly less than those achieved from the combinations, with the RFP medium cassettes indistinguishable from prediction and the RFP high cassettes consistently below prediction. In this experimental design, the three constructs (GFP, RFP, and BFP) were co-transformed on separate plasmids in order to minimize feedback from one expression cassette to the other; however, some of the variability between observed vs predicted results could be due to the energetic load placed on the cells. For example, one may hypothesize that maximal expression of GFP alone would be higher than when a cell is tasked with producing two other fluorescent proteins. This would be a simple mass balance problem, where each cell has a set capacity to produce heterologous proteins. The production of one protein thus has an effect on a cell's ability to produce another protein. In this situation, it would be anticipated that combinations with lower production capabilities (low and medium) would be most accurately predicted as they would be farthest from this maximal threshold. To test this hypothesis, it would be necessary to test low expressing constructs for all three fluorescent proteins and validate if the predictions are more accurate. Perhaps more importantly, in future works, the effect of one expression cassette on another in binary or ternary expression vectors should be tested, as this would be the likely scenario for the generation of transgenic plants.

All constructs analyzed maintained similar expression levels compared to predicted single cassette activities, with the exception of both low and medium expressing cassettes for BFP. As expected from the single cassette GFP experiments, high BFP expression was achieved from Combo-2 and Combo-5. Surprisingly, even higher expression was quantified from the predicted medium expressers Combo-3 and Combo-4. Though not higher than Combo-2 and Combo-5, high expression was also detected from the predicted low expressers Combo-1 and Combo-6. In these particular cases, it is possible that the promoter-5′UTR in the predicted low and medium expressing BFP cassettes combined with the downstream *mTag-BFP2* coding sequence to create a motif enhancing transgene expression. It is known that the nucleotide region surrounding the ATG start codon is important to create a favorable start codon, and downstream sequences after can also have an enhancing effect on expression and protein production.[45]

The data from the library described here represents a valuable tool to estimate and experimentally reproduce a known stoichiometry of expression for multi-component pathways. This investigation will accelerate metabolic engineering of complex heterologous pathways where the expression of

https://doi.org/10.1021/acssynbio.2c00147
ACS Synth. Biol. 2022, 11, 2741−2755

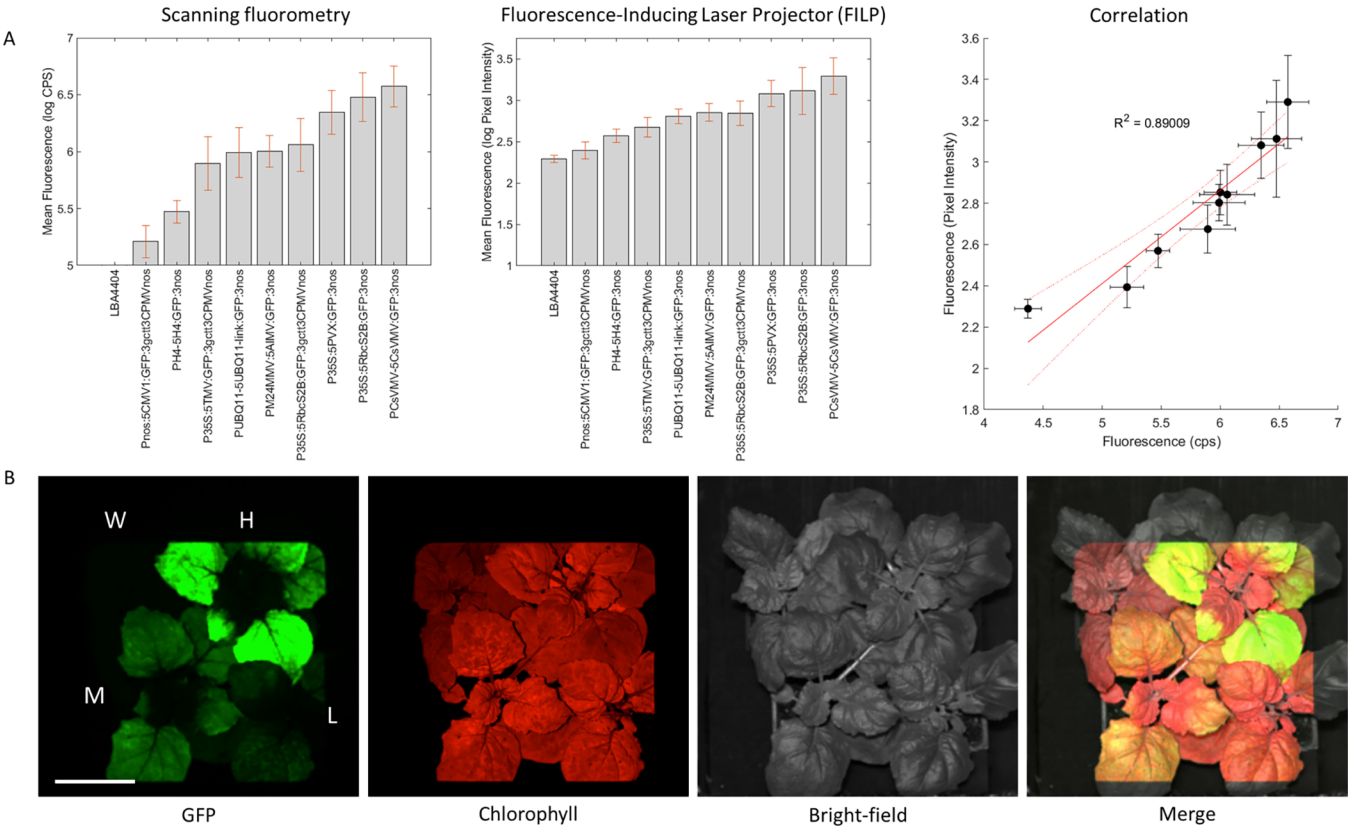

Figure 8. Analysis of the activity of genetic modules in canopies by a fluorescence-inducing laser projector (FILP). (A) Graphs represent fluorometric data obtained using intact leaf tissue. Scanning fluorometry (excitation 475 nm, emission 509 nm) data is expressed as $\log_{10}$ of CPS (counts per second) values, while FILP (Fluorescence-Inducing Laser Projector) (excitation 465, 525 nm, emission 525, 680 nm filters) data is expressed as $\log_{10}$ of pixel intensity. Data of the graph correlating both methods is also shown (R^2: ~0.89). Data is represented as the mean ± standard deviation (SD) of at least three transformed plants per construct. Plants expressing single high (H1−3: PCsVMV-5CsVMV:GFP:3*nos*, P35S:5RbcS2B:GFP:3*nos*, and P35S:5PVX:GFP:3*nos*), medium (M1−3:P35S:5RbcS2B:GFP:3gctt3CPMV*nos*, PM24MMV:5AIMV:GFP:3*nos*, and PUBQ11-5UBQ11-link:GFP:3*nos*), and low (L1−3: P35S:5TMV:GFP:3gctt3CPMV*nos*, PH4:5H4:GFP:3*nos*, and P*nos*:5CMV1:GFP:3gctt3CPMV*nos*) expression cassettes (Table S2) have been analyzed using the two methods. (B) FILP images showing *N. benthamiana* plants expressing high (H), medium (M), and low (L) expression cassettes along with wild-type controls (W). GFP (green), chlorophyll (red), bright-filed (gray), and merge images are shown. Scale bar: 10 cm.

a number of genes must be coordinated both within the pathway and in the endogenous cellular system. However, as seen with the BFP expressing cassettes, unpredicted motifs may originate and affect gene expression. Combinations of chosen regulatory elements with desired coding sequences must be tested and quantified in order to avoid unpredicted effects.

Analysis of Expression Cassettes in Canopies by Fluorescence-Inducing Laser Projector (FILP). Fluorescent signal produced by the canopy *N. benthamiana* plants infiltrated with low, medium, and high expresser cassettes was further analyzed using the fluorescence-inducing laser projector (FILP) standoff detection system.[46] Based on MEFL flow-cytometry data, the constructs were subdivided into high (MEFL: above 7 units), medium (MEFL: 6.5−7 units), and low (MEFL: 5−6.5 units) expressers. Three construct candidates per functional group were selected. The GFP and endogenous control pigment chlorophyll were imaged at a distance of 3 m. The GFP signal produced by the plant canopy was quantified by pixel intensity, and the chlorophyll signal was used to set the leaf area of each plant analyzed. The images in Figure 8 indicate that the three functional groups of constructs can be efficiently discriminated using this standoff detection system. This is supported by the high correlation (R^2 = 0.89) between pixel intensity values obtained using FILP and the corresponding fluorometric values obtained from the same leaf tissue. This high correlation is likely because values obtained using either technique are both representative of pooled-cell populations of intact tissues. These experiments confirmed that by modulating genetic regulatory elements, we could alter the level of fluorescent signal detectable at a distance of 3 m. Standoff detection is a necessary characteristic for engineered plants that sense and report the presence of environmental stimuli, termed phytosensors. It is crucial for these phytosensors to reach distinct expression levels between situations with or without the presence of the stimuli of interest. In the new era of plant synthetic biology, phytosensors will find important applications both in agriculture and human environments to monitor the presence of pathogens, chemicals, and physical stresses.[14,47]

CONCLUSIONS

The correlation between fluorometric values obtained from plant tissue and single cell analysis supports the quantified expression level from tested cassettes. Discrepancies between scanning fluorometry and flow cytometry data may be explained by the method of collection. While flow cytometry pools the data from ~10^6 individual various cell types, our

https://doi.org/10.1021/acssynbio.2c00147
ACS Synth. Biol. 2022, 11, 2741−2755

scanning fluorometer collects ≤3 technical replicates from arbitrary spots on a leaf to quantify expression for a population of cells. Additionally, it is possible that threshold detection limits may be different for either instrument. It is evident that our current methods for flow cytometry do not accurately quantify expression from weaker constructs. This may seem counter-intuitive, as flow cytometry is typically more sensitive to low expression levels than bulk measurement methods but is caused in this case by challenges in the effective gating of a heterogeneous sample event population. Additional studies can likely tune the sensitivity for flow cytometry by adjusting sample preparation and data gating methods in order to better enrich the events of interest in the assay and thus improve the limit of detection. Regardless, the relatively fast time to acquire expression data from leaves is enough to roughly predict values obtained by both standoff detection of plant canopies and single cell analysis, and even this rough level of agreement across multiple instruments increases the degree of confidence that can be taken in the values that are reported. Furthermore, the calibration of flow cytometry data to units of equivalent standard dye molecules allows reproducible measurements of the activity of plant regulatory elements across different laboratories, as well as meaningful data interpretation and modeling with respect to the actual molecular biology of the cells. The typical use of arbitrary or relative units for reporting fluorescence, by contrast, is a source of high uncertainty when data is compared across different laboratories or experiments. Likewise, calibrated flow cytometry also provides a path for linking the counts-per-second of the Fluorolog, pixel intensity units of standoff detection, and molecular interpretation of phenomena being quantified.

Building on these results, standard laboratory equipment such as a plate reader could likely be used for rapid quantification in labs without a Fluorolog-3 scanning fluorometer. Likewise, data collection from flow cytometry for prediction software could be utilized to predict the canopy expression level necessary for standoff detection. Single cell analysis allows for large sets of quantitative data to be calculated from a population of cells. In comparison with the analysis of intact tissue, flow cytometry allows more robust statistical parameters calculated on $\sim 10^6$ events. Furthermore, protoplasts extracted from various tissues reflect data on different cell subpopulations. This information is important to compile a plant cell atlas, allowing users to analyze and subdivide cells depending on size, internal complexity, and fluorescence level. The plant synthetic biology community will tremendously benefit from a common resource of activity of genetic modules, allowing more precise, reproducible, and predictable engineering of plant cells.

Through the use of these three methods, we improved the available knowledge regarding activity of regulatory elements and initiated the process of prediction, from single cell to leaf and canopy expression. This is important in the context of phenomics, where information at genetic levels is associated to plant attributes. With regard to engineered plants used to sense environmental stimuli (phytosensors), the quantified level of fluorescence from standoff detection is particularly important. These phytosensors must be optimally designed to prevent false positive or false negative reporting of potentially harmful detected stimuli. Through the use of this library, the on/off state of phytosensors can be properly tuned for realistic function.

The library described here is only one of the first steps toward building a foundation of knowledge for plant synthetic biology. Several additional kinds of studies will help assemble a comprehensive rulebook. (1) The regulatory elements described in this work clearly do not encompass all possible modules available for plant transgene expression. Many other promoters, UTRs, N and C-terminal tags, linkers, and other types of modules could be designed, assembled, and analyzed. Additionally, monocotyledon regulatory elements are not typically functional in dicotyledon plants. Additional studies focusing on monocotyledon parts will be necessary to expand described libraries to this other group of flowering plants. (2) Scars resulting from molecular cloning can have considerable effects on transgene expression. Here, we demonstrated that four base pair sequences between the stop codon and 3′UTR have dramatic effects on gene expression. With regard to Golden Gate cloning, screening of all 256 possible four-nucleotide overhangs used to link modules could be used to optimize this method. However, utilizing insulators or modeling approaches, similar to what has been achieved in other organisms, will provide a more robust solution, especially when considering the varying effects of different genes of interest and not just well-characterized reporters. (3) It is known that potentially deleterious positional effects occur following transgene integration into the plant genome.[48] It is likely that positional effects also occur from the spacing and orientation of multiple transgene cassettes in transformation vectors. Therefore, the evaluation of respective cassettes' expressions due to different structural designs and orientations will be important to perform precise metabolic engineering. Unpredicted genetic motifs with strong effects on gene expression can occur when combining different regulatory elements. The validation of novel combined modules with unique expression patterns will considerably expand the library of genetic parts.

There are undoubtedly additional kinds of studies that would continue to advance the overall goal of plant synthetic biology. Likely, many of these studies could be conducted in a manner similar to the one described here. Regardless, there are improvements necessary for high-throughput screening of increasingly populated module libraries. Though beneficial and appropriate for state-of-the-art plant biotechnology, agro-infiltration of *N. benthamiana* is hindered by the need for hands-on labor. PEG-mediated transfection of protoplasts by robotics seems to be the most likely answer to this high-throughput bottleneck.[49] Protoplasts can easily be obtained in large numbers through the generation of cell suspension cultures.[21] Though established methods have been generated for robotics transfection of protoplasts, a potential hurdle is the necessity of concentrated and purified plasmid DNA.[50] To overcome this necessity, protocols could be potentially established describing the use of PCR products for transformation, as opposed to plasmids. Nonetheless, agroinfiltration is a currently accepted method for transient expression of transgenes in plants and can be immediately conducted to screen module libraries to progress the molecular toolbox. Studies such as this one will help the long-term goal of synthetic biology to develop new plants to secure and sustain a growing human population.

MATERIALS AND METHODS

Plant Growth Conditions. *Nicotiana benthamiana* plants were grown on a BK25 potting mix (ProMix) for 4−6 weeks

https://doi.org/10.1021/acssynbio.2c00147
ACS Synth. Biol. 2022, 11, 2741−2755

before *Agrobacterium tumefaciens*-mediated transformation. Plants were kept in a controlled environment at a constant temperature of 24 °C and a light/dark cycle of 16/8 h, respectively. Irradiation was provided using LED light at an intensity of ∼350 μmol m^{-2} s^{-1}. After transformation, plants were kept at the same environmental conditions listed before.

Construction of Plant Transformation Vectors. Golden Gate modular cloning was used to assemble plant transformation vectors as previously described.[20,26] The IIS restriction enzymes *Bsa*I-HF-V2 (New England Biolabs, NEB) and *Bpi*I (Anza Invitrogen, Thermo Fisher Scientific) were used for level-1 and level-2 assemblies, respectively. All modules used for Golden Gate assembly have been designed and domesticated as previously described.[20,26] A list of genetic regulatory elements including promoters, 5′UTRs, 3′UTRs, and coding sequences used in this study is shown in Table S1. The coding sequences for GFP (mEmerald) (FPbase ID: AD4BK), BFP (mTag-BFP2) (FPbase ID: ZO7NN), and RFP (mScarlet-I) (FPbase ID: 6VVTK) were gene synthesized through GeneArt (Thermo Fisher Scientific). Plant expression cassettes for testing regulatory elements were integrated into the level-2 acceptor plasmid pAGM4723.[26]

Vacuum Infiltration of *N. Benthamiana* Plants. The library of plant transformation vectors generated in this study was transformed in *A. tumefaciens* LBA4404 by using the freeze thawing method as described previously.[51] For plant transformation, a single bacteria colony carrying the construct of interest was grown overnight in YEP selective liquid media (10 g/L peptone; 10 g/L yeast extract; 5 g/L NaCl; 50 mg/L rifampicin; 50 mg/L kanamycin; pH 7) at 28 °C under vigorous shaking (250 rpm). The day after, 1 mL of preculture was inoculated in 100 mL of fresh YEP selective liquid media. After 24 h of growth at the same conditions, 100 μL of 100 mM acetosyringone was added, and then the culture was grown for an extra hour. Bacterial cells were pelleted by centrifugation at 4000*g* for 10 min at room temperature and resuspended in infiltration buffer (10 mM 2-(*N*-morpholino)-ethanesulfonic acid hydrate, MES pH 5.7; 10 mM $MgCl_2$; 100 μM acetosyringone) to an OD of 0.6 for all single constructs tested. For the combination infiltrations of three different cassettes, they were each mixed at 0.2 OD, reaching a final OD of 0.6. Each plant infiltration requires ∼300 mL of bacteria solution. The bacteria solution was poured in a Magenta GA-7 vessel (7.7 × 7.7 × 9.7 cm size) able to contain the entire canopy of 4−6-week-old plants. After submersion into the bacteria solution, the plant infiltration was performed in a chamber applying and releasing vacuum for 3−6 times until complete infiltration. Infiltrated leaves were pat dried to remove the excess bacterial solution, returned to a controlled environment, and analyzed 72 h post infiltration. A minimum of three plants were infiltrated per construct.

Fluorometric Analysis of Leaves. The scanning fluorescence spectroscopy apparatus (Fluorolog-3, Jobin Yvon and Glen Spectra, Edison, NJ) equipped with the FluorEssence Software (HORIBA Scientific, version 3.8.0.60) was used to quantify the fluorometric signal from leaf tissue as described previously.[46] The GFP, RFP, and BFP signals were analyzed at excitation wavelengths of 475, 550, and 400 nm, and emission ranges of 509, 574, and 455 nm, respectively, to collect the maximum emission peaks. Six measurements per infiltrated plant were collected from the same leaf tissue used for protoplasts isolation. A minimum of three independent plants per construct was analyzed. Fluorometric data was processed using Microsoft Excel software as previously described.[46] The results are expressed as mean ± standard deviation of $\log_{10}$ of CPS (counts per second). To ensure that detected fluorescence was not the direct result of *A. tumefaciens*, cultures containing constructs with promoters and 5′ UTRs from *A. tumefaciens* were checked for expression on a plate reader (Figure S2).

Protoplasts Isolation. The top three fully expanded leaves of each agroinfiltrated plant were cut into strips of 2−3 mm width using a blade. Leaf tissue was then put in a deep Petri dish (10 cm diameter and 2 cm height) containing 25 mL of freshly made enzyme solution (600 mM mannitol; 1 mg/mL BSA; 20 mM KCl; 10 mM $CaCl_2$; 4.6 mM β-mercaptoethanol; 20 mM 2-(*N*-morpholino)ethanesulfonic acid hydrate, MES pH 5.7; along with 24 μL of Rohament CL; 22 μL of Rohapect 10 L and 2.2 μL of Rohapect UF per each ml of solution) and incubated in the dark under gentle shaking (40−50 rpm) at room temperature for 2−3 h. After this incubation time, the plates were incubated for 5 extra minutes at 80 rpm shaking to facilitate the release of protoplasts from digested leaf tissue. The protoplast solution was then filtered through a 40 μm nylon mesh filter into a clean Petri dish. After transferring into a 50 mL conical tube, filtrated protoplasts were centrifuged at 100 × *g* for 3 min and then the cell pellet was resuspended in 5 mL of washing solution (600 mM mannitol; 20 mM KCl; 4 mM 2-(*N*-morpholino)ethanesulfonic acid hydrate, MES pH 5.7). The protoplast solution was underlaid with 5 mL of 23% sucrose, keeping the two phases separated. After centrifugation at 100 × *g* for 3 min, 5−6 mL of live protoplasts were collected at the interface sucrose/washing solution. Protoplasts were diluted adding 8−10 mL of fresh wash buffer in a 15 mL tube, centrifuged again at 100 × *g* for 3 min, and then the cell pellet was resuspended in 1−2 mL of incubation solution (500 mM mannitol; 20 mM KCl; 4 mM 2-(*N*-morpholino)-ethanesulfonic acid hydrate, MES pH 5.7). Resuspended protoplasts were then analyzed by flow cytometry.

Flow Cytometry and Data Analysis. Flow cytometric analysis was conducted using an Attune NxT acoustic focusing cytometer equipped with the manufacturer's operating software (Life Technologies, Carlsbad, CA, USA). Protoplasts suspended in WI buffer at a concentration of ∼1 × 10^5 cells per mL were analyzed at an acquisition volume of 750 μL with a flow rate of 500 μL/min. Forward-scattered (FSC) and side-scattered (SSC) light voltages were set at 50 and 180 V, respectively. The GFP, BFP, and RFP fluorescent reporters were excited using 488, 405, and 561 nm lasers with 510/10, 440/50, and 585/16 bandpass filters, respectively. The voltage for GFP was 200 V, whereas those for BFP and RFP were at 300 V.

Flow cytometry data was processed using the TASBE Flow Analytics software package,[52] using the recommended practices for gating, background subtraction, and bead-based calibration, using the closest-fit match of GFP to the defined 488 excitation and 530/30 filter channel for MEFL units on SpheroTech URQP-38-6 K calibration beads. Data from each sample was fit to a two-component Gaussian mixture, with the low component interpreted as non-transfected cells and the high component interpreted as transfected cells. The non-transfected component was discarded, and statistics for the high component was reported. Additional details and examples are provided in the Supporting Information, "Flow Cytometry Data Processing". The results are expressed as the mean ±

https://doi.org/10.1021/acssynbio.2c00147
ACS Synth. Biol. 2022, 11, 2741−2755

standard deviation of $\log_{10}$ of MEFL (molecules of equivalent fluorescein).

Fluorescence-Inducing Laser Projector (FILP) Imaging. The fluorescence-inducing laser projector (FILP) was used for imaging agroinfiltrated *N. benthamiana* canopies expressing fluorescent reporters as described previously.[46] The GFP fluorescent signal was acquired at 100 ms of exposure time using a 465 nm laser and a 525 nm emission filter, while the chlorophyll a was imaged at 100 ms of exposure time using a 525 nm emission laser and detected using a 680 nm filter. The standoff detection was performed at 3 m from the laser source.

Images were processed using ImageJ 1.41o (National Institute of Health, Bethesda, MD, USA), and the same software was used to quantify the fluorescence intensity from plant canopies. For this purpose, chlorophyll images were used to set the threshold and automatically identify individual canopy areas (ROI: region of interest), and then the GFP fluorescence in these regions of interests was quantified by pixel intensity. The results are expressed as the mean ± standard deviation of $\log_{10}$ of pixel intensity.

Confocal Microscopy. Agroinfiltrated *Nicotiana benthamiana* leaves were imaged using an Olympus Fv1000 confocal microscope (Olympus) equipped with argon, HeNe, and diode lasers. The mEmerald, mTag-BFP2, and mScarlet-I fluorescent proteins were detected at optimal excitation (Ex)/emission (Em) wavelengths of 487/509, 399/454 and 569/593, respectively. Chlorophyll was excited at a wavelength of 561 nm and detected at 682 nm. Digital images were acquired using the Olympus FV10-ASW Viewer software Ver.4.2a (Olympus) and processed using ImageJ 1.41o (National Institute of Health, Bethesda, MD, USA).

Expression Analysis. We do not use significance testing methods because our aim is to evaluate quantitative levels of expression, not to test a hypothesis about differences of distributions. Significance testing is therefore not applicable: each set of samples may be evaluated independently in terms of how well its expression level has been able to be determined, as shown through the geometric mean, geometric standard deviation, and (for flow cytometry) the geometric means for individual samples. Note also that such statistics have previously been shown to be effective for modeling and prediction of genetic regulatory elements.[24,53−55]

AUTHOR CONTRIBUTION

A.C.P., A.O., M.-A.N., H.S., C.N.S., J.B., and S.C.L. designed the strategy; A.C.P., A.O., M.-A.N., L.T.D., S.A.H., L.L., D.N.R., and T.M.S. collected data; A.C.P., A.O., M.-A.N., and H.S. analyzed data; A.C.P., A.O., M.-A.N., H.S., C.N.S., J.B., and S.C.L. wrote the article.

ASSOCIATED CONTENT

Supporting Information

The Supporting Information is available free of charge at https://pubs.acs.org/doi/10.1021/acssynbio.2c00147.

(Figure S1) Further fluorometric analysis on the effect of a four base pair scar, between the stop codon and the 3′UTR, on gene expression; (Figure S2) data demonstrating that the promoters used in this work are not functional in the *Agrobacterium* host; expanded detail on the procedures used to process the flow cytometry data; figures providing prototypical examples of the output from each of the data processing steps (PDF)

(Table S1) nucleotide sequence and a brief description for all regulatory elements and genes of interest used in this study; (Table S2) information on the constructs assembled and tested in this work and key for construct naming (PDF)

Comparative analysis of different 4 base pair scars between the stop codon and the 3′UTR (PDF)

Expression of GFP by *Agrobacterium A. tumefaciens* strain LBA4404 cultures transfected with plasmids (PDF)

AUTHOR INFORMATION

Corresponding Author

Scott C. Lenaghan − *Department of Food Science, University of Tennessee Knoxville, Knoxville, Tennessee 37996, United States; Center for Agricultural Synthetic Biology, University of Tennessee Institute of Agriculture, Knoxville, Tennessee 37996, United States;* orcid.org/0000-0002-7539-1726; Email: slenagha@utk.edu

Authors

Alexander C. Pfotenhauer − *Department of Food Science, University of Tennessee Knoxville, Knoxville, Tennessee 37996, United States; Center for Agricultural Synthetic Biology, University of Tennessee Institute of Agriculture, Knoxville, Tennessee 37996, United States*

Alessandro Occhialini − *Department of Food Science, University of Tennessee Knoxville, Knoxville, Tennessee 37996, United States; Center for Agricultural Synthetic Biology, University of Tennessee Institute of Agriculture, Knoxville, Tennessee 37996, United States*

Mary-Anne Nguyen − *Department of Food Science, University of Tennessee Knoxville, Knoxville, Tennessee 37996, United States; Center for Agricultural Synthetic Biology, University of Tennessee Institute of Agriculture, Knoxville, Tennessee 37996, United States*

Helen Scott − *Intelligent Software and Systems, Raytheon BBN Technologies, Cambridge, Massachusetts 02138, United States*

Lezlee T. Dice − *Department of Food Science, University of Tennessee Knoxville, Knoxville, Tennessee 37996, United States; Center for Agricultural Synthetic Biology, University of Tennessee Institute of Agriculture, Knoxville, Tennessee 37996, United States*

Stacee A. Harbison − *Department of Food Science, University of Tennessee Knoxville, Knoxville, Tennessee 37996, United States; Center for Agricultural Synthetic Biology, University of Tennessee Institute of Agriculture, Knoxville, Tennessee 37996, United States*

Li Li − *Department of Food Science, University of Tennessee Knoxville, Knoxville, Tennessee 37996, United States; Center for Agricultural Synthetic Biology, University of Tennessee Institute of Agriculture, Knoxville, Tennessee 37996, United States*

D. Nikki Reuter − *Department of Food Science, University of Tennessee Knoxville, Knoxville, Tennessee 37996, United States; Center for Agricultural Synthetic Biology, University of Tennessee Institute of Agriculture, Knoxville, Tennessee 37996, United States*

Tayler M. Schimel − *Department of Food Science, University of Tennessee Knoxville, Knoxville, Tennessee 37996, United States; Center for Agricultural Synthetic Biology, University of*

https://doi.org/10.1021/acssynbio.2c00147
ACS Synth. Biol. 2022, 11, 2741−2755

Tennessee Institute of Agriculture, Knoxville, Tennessee 37996, United States

C. Neal Stewart, Jr − *Center for Agricultural Synthetic Biology, University of Tennessee Institute of Agriculture, Knoxville, Tennessee 37996, United States; Department of Plant Sciences, University of Tennessee Knoxville, Knoxville, Tennessee 37996, United States*

Jacob Beal − *Intelligent Software and Systems, Raytheon BBN Technologies, Cambridge, Massachusetts 02138, United States*

Complete contact information is available at: https://pubs.acs.org/10.1021/acssynbio.2c00147

Author Contributions

#A.C.P. and A.O. contributed equally.

Notes

The authors declare no competing financial interest.

■ ACKNOWLEDGMENTS

This work was supported by Air Force Research Laboratory (AFRL) and DARPA contracts FA8750-17-C-0184 and HR0011-18-2-0049. This document does not contain technology or technical data controlled under either U.S. International Traffic in Arms Regulation or U.S. Export Administration Regulations. Views, opinions, and/or findings expressed are those of the author(s) and should not be interpreted as representing the official views or policies of the Department of Defense or the U.S. Government.

■ ABBREVIATIONS

FILP, fluorescence-inducing laser projector; MEFL, molecules of equivalent fluorescein; 5′ & 3′UTR, untranslated region at either 5′ or 3′ end

■ REFERENCES

(1) Smith, P.; Gregory, P. J. Climate change and sustainable food production. *Proc. Nutr. Soc.* **2013**, *72*, 21−28.

(2) Bailey-Serres, J.; Parker, J. E.; Ainsworth, E. A.; Oldroyd, G. E. D.; Schroeder, J. I. Genetic strategies for improving crop yields. *Nature* **2019**, *575*, 109−118.

(3) Occhialini, A.; Lin, M. T.; Andralojc, P. J.; Hanson, M. R.; Parry, M. A. Transgenic tobacco plants with improved cyanobacterial Rubisco expression but no extra assembly factors grow at near wild-type rates if provided with elevated CO_2. *Plant J.* **2016**, *85*, 148−160.

(4) Fitch, M. M. M.; Manshardt, R. M.; Gonsalves, D.; Slightom, J. L.; Sanford, J. C. Virus resistant papaya plants derived from tissues bombarded with the coat protein gene of papaya ringspot virus. *Nat. Biotechnol.* **1992**, *10*, 1466−1472.

(5) Castiglioni, P.; Warner, D.; Bensen, R. J.; Anstrom, D. C.; Harrison, J.; Stoecker, M.; Abad, M.; Kumar, G.; Salvador, S.; D'Ordine, R.; Navarro, S.; Back, S.; Fernandes, M.; Targolli, J.; Dasgupta, S.; Bonin, C.; Luethy, M. H.; Heard, J. E. Bacterial RNA chaperones confer abiotic stress tolerance in plants and improved grain yield in maize under water-limited conditions. *Plant Physiol.* **2008**, *147*, 446−455.

(6) Qi, B.; Fraser, T.; Mugford, S.; Dobson, G.; Sayanova, O.; Butler, J.; Napier, J. A.; Stobart, A. K.; Lazarus, C. M. Production of very long chain polyunsaturated omega-3 and omega-6 fatty acids in plants. *Nat. Biotechnol.* **2004**, *22*, 739−745.

(7) Ye, X.; Al-Babili, S.; Klöti, A.; Zhang, J.; Lucca, P.; Beyer, P.; Potrykus, I. Engineering the provitamin A (β-carotene) biosynthetic pathway into (carotenoid-free) rice endosperm. *Science* **2000**, *287*, 303−305.

(8) Butelli, E.; Titta, L.; Giorgio, M.; Mock, H.-P.; Matros, A.; Peterek, S.; Schijlen, E. G.; Hall, R. D.; Bovy, A. G.; Luo, J.; Martin, C. Enrichment of tomato fruit with health-promoting anthocyanins by expression of select transcription factors. *Nat. Biotechnol.* **2008**, *26*, 1301−1308.

(9) Raffan, S.; Sparks, C.; Huttly, A.; Hyde, L.; Martignago, D.; Mead, A.; Hanley, S. J.; Wilkinson, P. A.; Barker, G.; Edwards, K. J.; Curtis, T. Y.; Usher, S.; Kosik, O.; Halford, N. G. Wheat with greatly reduced accumulation of free asparagine in the grain, produced by CRISPR/Cas9 editing of asparagine synthetase gene *TaASN2*. *Plant Biotechnol. J.* **2021**, *19*, 1602−1613.

(10) Zhu, X. G.; Ort, D. R.; Parry, M. A. J.; von Caemmerer, S. A wish list for synthetic biology in photosynthesis research. *J. Exp. Bot.* **2020**, *71*, 2219−2225.

(11) Vicente, E. J.; Dean, D. R. Keeping the nitrogen-fixation dream alive. *PNAS* **2017**, *114*, 3009−3011.

(12) Liu, W.; Yuan, J. S.; Stewart, C. N., Jr. Advanced genetic tools for plant biotechnology. *Nat. Rev. Genet.* **2013**, *14*, 781−793.

(13) Caddick, M. X.; Greenland, A. J.; Jepson, I.; Krause, K.-P.; Qu, N.; Riddell, K. V.; Salter, M. G.; Schuch, W.; Sonnewald, U.; Brian Tomsett, A. An ethanol inducible gene switch for plants used to manipulate carbon metabolism. *Nat. Biotechnol.* **1998**, *16*, 177−180.

(14) Aoyama, Y.; Chua, N.-H. A glucocorticoid-mediated transcriptional induction system in transgenic plants. *Plant J.* **1997**, *11*, 605−612.

(15) Lescot, M.; Déhais, P.; Thijs, G.; Marchal, K.; Moreau, Y.; Peer, Y. V.; Rouzé, P.; Rombauts, S. PlantCARE, a database of plant *cis*-acting regulatory elements and a portal to tools for *in silico* analysis of promoter sequences. *Nucleic Acids Res.* **2002**, *30*, 325−327.

(16) Kwon, C. S.; Paek, K. H.; Chung, W. I. The 5′ untranslated region of cucumber mosaic virus RNA4 confers highly competitive activity on heterologous luciferase mRNA in cell-free translation. *FEBS Lett.* **1998**, *422*, 89−93.

(17) Meshcheriakova, Y. A.; Saxena, P.; Lomonossoff, G. P. Fine-tuning levels of heterologous gene expression in plants by orthogonal variation of the untranslated regions of a nonreplicating transient expression system. *Plant Biotechnol. J.* **2014**, *12*, 718−727.

(18) Phoolcharoen, W.; Bhoo, S. H.; Lai, H.; Ma, J.; Arntzen, C. J.; Chen, Q.; Mason, H. S. Expression of an immunogenic Ebola immune complex in *Nicotiana benthamiana*. *Plant Biotechnol. J.* **2011**, *9*, 807−816.

(19) Mason, H. S.; Lam, D. M.; Arntzen, C. J. Expression of hepatitis B surface antigen in transgenic plants. *PNAS* **1992**, *89*, 11745−11749.

(20) Occhialini, A.; Piatek, A. A.; Pfotenhauer, A. C.; Frazier, T. P.; Stewart, C. N., Jr.; Lenaghan, S. C. MoChlo: a versatile, modular cloning toolbox for chloroplast biotechnology. *Plant Physiol.* **2019**, *179*, 943−957.

(21) Sultana, M. S.; Frazier, T. P.; Millwood, R. J.; Lenaghan, S. C.; Stewart, C. N., Jr. Development and validation of a novel and robust cell culture system in soybean (*Glycine max* (L.) Merr.) for promoter screening. *Plant Cell Rep.* **2019**, *38*, 1329−1345.

(22) Hoffman, R. A.; Wang, L.; Bigos, M.; Nolan, J. P. NIST/ISAC standardization study: variability in assignment of intensity values to fluorescence standard beads and in cross calibration of standard beads to hard dyed beads. *Cytometry A.* **2012**, *81A*, 785−796.

(23) Beal, J.; Haddock-Angelli, T.; Baldwin, G.; Gershater, M.; Dwijayanti, A.; Storch, M.; de Mora, K.; Lizarazo, M.; Rettberg, R.; with the iGEM Interlab Study Contributors. Quantification of bacterial fluorescence using independent calibrants. *PLoS One* **2018**, *13*, No. e0199432.

(24) Beal, J.; Wagner, T. E.; Kitada, T.; Azizgolshani, O.; Parker, J. M.; Densmore, D.; Weiss, R. Model-driven engineering of gene expression from RNA replicons. *ACS Synth. Biol.* **2015**, *4*, 48−56.

(25) Weinberg, B. H.; Cho, J. H.; Agarwal, Y.; Pham, N. T. H.; Caraballo, L. D.; Walkosz, M.; Ortega, C.; Trexler, M.; Tague, N.; Law, B.; Benman, W. K. J.; Letendre, J.; Beal, J.; Wong, W. W. High-performance chemical- and light-inducible recombinases in mammalian cells and mice. *Nat. Commun.* **2019**, *10*, 4845.

(26) Engler, C.; Youles, M.; Gruetzner, R.; Ehnert, T.-M.; Werner, S.; Jones, J. D. G.; Patron, N. J.; Marillonnet, S. A Golden Gate

modular cloning toolbox for plants. *ACS Synth. Biol.* **2014**, *3*, 839−843.
(27) Odell, J. T.; Nagy, F.; Chua, N. H. Identification of DNA sequences required for activity of the cauliflower mosaic virus 35S promoter. *Nature* **1985**, *313*, 810−812.
(28) Fang, R. X.; Nagy, F.; Sivasubramaniam, S.; Chua, N. H. Multiple *cis* regulatory elements for maximal expression of the cauliflower mosaic virus 35S promoter in transgenic plants. *Plant Cell* **1989**, *1*, 141−150.
(29) Kay, R.; Chan, A.; Daly, M.; McPherson, J. Duplication of CaMV 35S promoter sequences creates a strong enhancer for plant genes. *Science* **1987**, *236*, 1299−1302.
(30) Ow, D. W.; Jacobs, J. D.; Howell, S. H. Functional regions of the cauliflower mosaic virus 35S RNA promoter determined by use of the firefly luciferase gene as a reporter of promoter activity. *PNAS* **1987**, *84*, 4870−4874.
(31) Cai, Y. M.; Kallam, K.; Tidd, H.; Gendarini, G.; Salzman, A.; Patron, N. J. Rational design of minimal synthetic promoters for plants. *Nucleic Acids Res.* **2020**, *48*, 11845−11856.
(32) Jores, T.; Tonnies, J.; Wrightsman, T.; Buckler, E. S.; Cuperus, J. T.; Fields, S.; Queitsch, C. Synthetic promoter designs enabled by a comprehensive analysis of plant core promoters. *Nat. Plants* **2021**, *7*, 842−855.
(33) Ingelbrecht, I. L.; Herman, L. M.; Dekeyser, R. A.; Van Montagu, M. C.; Depicker, A. G. Different 3′ end regions strongly influence the level of gene expression in plant cells. *Plant Cell* **1989**, *1*, 671−680.
(34) An, Y. Q.; McDowell, J. M.; Huang, S.; McKinney, E. C.; Chambliss, S.; Meagher, R. B. Strong, constitutive expression of the *Arabidopsis ACT2/ACT8* actin subclass in vegetative tissues. *Plant J.* **1996**, *10*, 107−121.
(35) Barker, R. F.; Idler, K. B.; Thompson, D. V.; Kemp, J. D. Nucleotide sequence of the T-DNA region from the *Agrobacterium tumefaciens* octopine Ti plasmid pTi15955. *Plant Mol. Biol.* **1983**, *2*, 335−350.
(36) Samac, D. A.; Tesfaye, M.; Dornbusch, M.; Saruul, P.; Temple, S. J. A comparison of constitutive promoters for expression of transgenes in alfalfa (*Medicago sativa*). *Transgenic Res.* **2004**, *13*, 349−361.
(37) Govindarajulu, M.; Elmore, J. M.; Fester, T.; Taylor, C. G. Evaluation of constitutive viral promoters in transgenic soybean roots and nodules. *Mol. Plant-Microbe Interact.* **2008**, *21*, 1027−1035.
(38) Norris, S. R.; Meyer, S. E.; Callis, J. The intron of *Arabidopsis thaliana* polyubiquitin genes is conserved in location and is a quantitative determinant of chimeric gene expression. *Plant Mol. Biol.* **1993**, *21*, 895−906.
(39) Potenza, C.; Aleman, L.; Sengupta-Gopalan, C. Targeting transgene expression in research, agricultural, and environmental applications: promoters used in plant transformation. *In Vitro Cell Dev. Biol. Plant* **2004**, *40*, 1−22.
(40) Chiba, Y.; Green, P. J. mRNA degradation machinery in plants. *J. Plant Biol.* **2009**, *52*, 114−124.
(41) Jackson, R. J.; Hellen, C. U. T.; Pestova, T. V. The mechanism of eukaryotic translation initiation and principles of its regulation. *Nat. Rev. Mol. Cell Biol.* **2010**, *11*, 113−127.
(42) Peyret, H.; Brown, J. K. M.; Lomonossoff, G. P. Improving plant transient expression through the rational design of synthetic 5′ and 3′ untranslated regions. *Plant Methods* **2019**, *15*, 108.
(43) Carr, S. B.; Beal, J.; Densmore, D. M. Reducing DNA context dependence in bacterial promoters. *PLoS One* **2017**, *12*, No. e0176013.
(44) Galdzicki, M.; Clancy, K. P.; Oberortner, E.; Pocock, M.; Quinn, J. Y.; Rodriguez, C. A.; Roehner, N.; Wilson, M. L.; Adam, L.; Anderson, J. C.; Bartley, B. A.; Beal, J.; Chandran, D.; Chen, J.; Densmore, D.; Endy, D.; Grünberg, R.; Hallinan, J.; Hillson, N. J.; Johnson, J. D.; Kuchinsky, A.; Lux, M.; Misirli, G.; Peccoud, J.; Plahar, H. A.; Sirin, E.; Stan, G. B.; Villalobos, A.; Wipat, A.; Gennari, J. H.; Myers, C. J.; Sauro, H. M. The Synthetic Biology Open Language (SBOL) provides a community standard for communicating designs in synthetic biology. *Nat. Biotechnol.* **2014**, *32*, 545−550.
(45) Sawant, S. V.; Kiran, K.; Singh, P. K.; Tuli, R. Sequence architecture downstream of the initiator codon enhances gene expression and protein stability in plants. *Plant Physiol.* **2001**, *126*, 1630−1636.
(46) Rigoulot, S. B.; Schimel, T. M.; Lee, J. H.; Sears, R. G.; Brabazon, H.; Layton, J. S.; Li, L.; Meier, K. A.; Poindexter, M. R.; Schmid, M. J.; Seaberry, E. M.; Brabazon, J. W.; Madajian, J. A.; Finander, M. J.; DiBenedetto, J.; Occhialini, A.; Lenaghan, S. C.; Stewart, C. N., Jr. Imaging of multiple fluorescent proteins in canopies enables synthetic biology in plants. *Plant Biotechnol. J.* **2020**, *19*, 830−843.
(47) Stewart, C. N., Jr.; Abudayyeh, R. K.; Stewart, S. G. Houseplants as home health monitors. *Science* **2018**, *361*, 229−230.
(48) Matzke, A. J.; Matzke, M. A. Position effects and epigenetic silencing of plant transgenes. *Curr. Opin. Plant Biol.* **1998**, *1*, 142−148.
(49) Lenaghan, S. C.; Neal Stewart, C., Jr. An automated protoplast transformation system. *Methods Mol. Biol.* **2019**, *1917*, 355−363.
(50) Dlugosz, E. M.; Lenaghan, S. C.; Stewart, C. N., Jr. A robotic platform for high-throughput protoplast isolation and transformation. *J. Visualized Exp.* **2016**, *27*, 54300.
(51) Weigel, D.; Glazebrook, J. Transformation of *agrobacterium* using the freeze-thaw method. *CSH Protoc.* **2006**, *2006*, pdb.prot4666.
(52) Beal, J.; Overney, C.; Adler, A.; Yaman, F.; Tiberio, L.; Samineni, M. TASBE Flow Analytics: a package for calibrated flow cytometry analysis. *ACS Synth. Biol.* **2019**, *8*, 1524−1529.
(53) Davidsohn, N.; Beal, J.; Kiani, S.; Adler, A.; Yaman, F.; Li, Y.; Xie, Z.; Weiss, R. Accurate predictions of genetic circuit behavior from part characterization and modular composition. *ACS Synth. Biol.* **2015**, *6*, 673−681.
(54) Wang, J.; Isaacson, S. A.; Belta, C. Modeling genetic circuit behavior in transiently transfected mammalian cells. *ACS Synth. Biol.* **2019**, *8*, 697−707.
(55) Kiwimagi, K. A.; Letendre, J. H.; Weinberg, B. H.; Wang, J.; Chen, M.; Watanabe, L.; Myers, C. J.; Beal, J.; Wong, W. W.; Weiss, R. Quantitative characterization of recombinase-based digitizer circuits enables predictable amplification of biological signals. *Commun. Biol.* **2021**, *4*, 1−12.

https://doi.org/10.1021/acssynbio.2c00147
ACS Synth. Biol. 2022, 11, 2741−2755